FEDERAL UNIVERSITY OF SANTA CATARINA

TECHNOLOGY CENTER

AUTOMATION AND SYSTEM DEPARTMENT

UNDERGRADUATE COURSE IN CONTROL AND AUTOMATION ENGINEERING

Yuri Schaupenlehner Haralamboff

Development of a DC-link current state observer for onboard charger Power Factor Correction

Toulouse, France

2023

Yuri Schaupenlehner Haralamboff

Development of a DC-link current state observer for onboard charger Power Factor Correction

Final report of the subject DAS5511 (Course Final Project) as a Concluding Dissertation of the Undergraduate Course in Control and Automation Engineering of the Federal University of Santa Catarina.
Supervisor: Prof. Max Hering de Queiroz, Dr.
Co-supervisor: Jérome Lachaize, Dr.

Toulouse, France

2023

Ficha de identificação da obra elaborada pelo autor, através do Programa de Geração Automática da Biblioteca Universitária da UFSC.

Yuri Schaupenlehner Haralamboff

**Development of a DC-link current state observer for onboard charger Power Factor
Correction**

This dissertation was evaluated in the context of the subject DAS5511 (Course Final Project)
and approved in its final form by the Undergraduate Course in Control and Automation
Engineering

Florianópolis, July 31th, 2023.

Prof. Hector Bessa Silveira, Dr.
Course Coordinator

Examing Board:

Prof. Jérome Lachaize, Dr.
Supervisor
Vitesco Technologies

Prof. Stephane Caux, Dr.
Evaluator
INP ENSEEIHT

Prof. Maurice Fadel, Dr.
Board President
INP ENSEEIHT

ACKNOWLEDGEMENTS

DISCLAIMER

Toulouse, July 31th, 2023.

As representative of the Vitesco Technologies in which the present work was carried out, I declare this document to be exempt from any confidential or sensitive content regarding intellectual property, that may keep it from being published by the Federal University of Santa Catarina (UFSC) to the general public, including its online availability in the Institutional Repository of the University Library (BU). Furthermore, I attest knowledge of the obligation by the author, as a student of UFSC, to deposit this document in the said Institutional Repository, for being it a Final Program Dissertation ("*Trabalho de Conclusão de Curso*"), in accordance with the *Resolução Normativa n° 126/2019/CUn*.

_____

Jérome Lachaize

Vitesco Technologies

ABSTRACT

As an alternative to the measurement of some variables in the engineering world by means of sensors, there are state observers as a cheaper financial solution and often more effective. Thus, to estimate the current entering a DC/DC converter of an on-board car battery charger, the Kalman Filter state observer is developed. In this monograph, three different methods of estimating the mentioned current are studied: only with the Kalman Filter, with the fusion of the estimation using the Kalman Filter together with an estimation with statistical bias and, finally, an estimation method only with the Kalman Filter but changing the initial state space of the system. Counting on the variation of some factors of the system to always work with the worst case of parameters in order to cover all cases of the systems within the 6σ area of statistics. Finally analyzing the results with Corner Case studies and also with Monte Carlo studies (following normal law of statistics for system parameters).

Keywords: Kalman Filter. Current estimation. DC/DC converter. Corner Case. Monte Carlo.

RESUMO

Como alternativa à medição de algumas grandezas no mundo da engenharia por meio de captores, existem os observadores de estados como uma solução mais barata financeiramente e muitas vezes mais efetiva. Desta forma, para estimar a corrente que entra em um conversor CC/CC de um carregador de bateria de carro embarcado, é desenvolvido o observador de estados Filtro de Kalman. Nesta monografia são estudados três métodos diferentes de estimação da corrente mencionada: somente com o Filtro de Kalman, com a fusão da estimação usando o Filtro de Kalman junto de uma estimação com viés estatístico e, por fim, um método de estimação somente com o Filtro de Kalman mas mudando o espaço de estados inicial do sistema. Contando com a variação de alguns fatores do sistema para trabalhar sempre com o pior caso de parâmetros com o objetivo de cobrir todos os casos dos sistemas dentro da área de 6σ da estatística. Por fim analisando os resultados com estudos de Corner Case e também com estudos de Monte Carlo (seguindo lei normal da estatística para os parâmetros do sistema).

Palavras-chave: Filtro de Kalman. Estimação corrente. Conversor CC/CC. Corner Case. Monte Carlo.

LIST OF FIGURES

CONTENTS

1 INTRODUCTION

1.1   THE ENTERPRISE

Vitesco Technologies is a fairly new company as its name first appears in 2019. In fact, this company is the Powertrain division of Continental, which changed its name to Vitesco Technologies.

Vitesco Technologies is headquartered in Regensburg, Germany. Today, Vitesco Technologies is a multinational company specializing in automotive equipment, with a focus on clean and sustainable mobility. It has more than 40,000 employees in nearly 50 locations.

Vitesco Technologies has 4 sites in France, the headquarters and the R&D center are located in Toulouse, in Boussens and in Foix are two production centers, and in Cergy the sales office.

Figure 1 – The four sites of Vitesco Technologies in France.
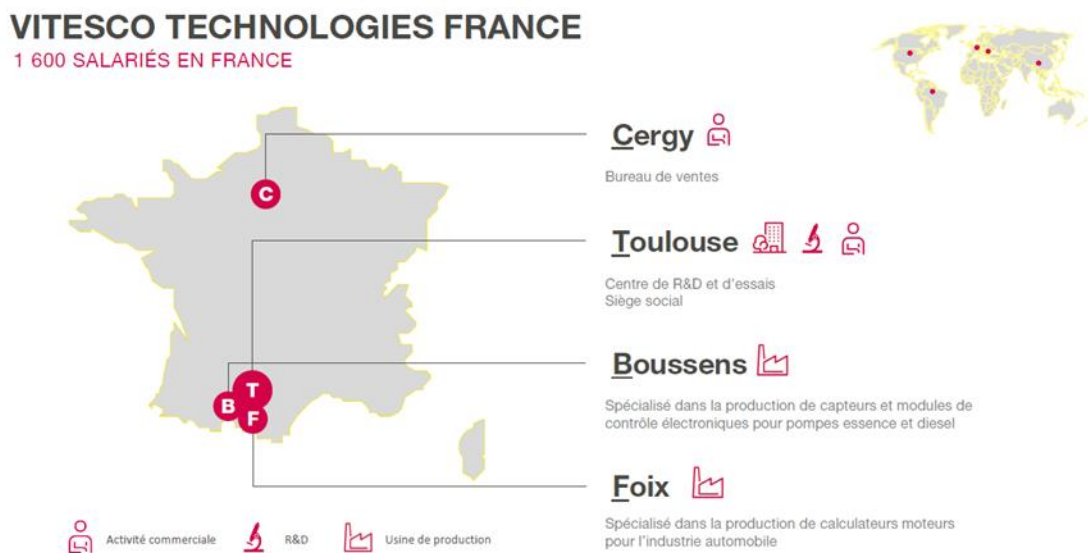
Source: Vitesco Technologies internal archives.

Four sites in France, Vitesco technologies has 1600 employees as shown on the infographic below:

Figure 2 – Diagram of the different power converters of the electric car.
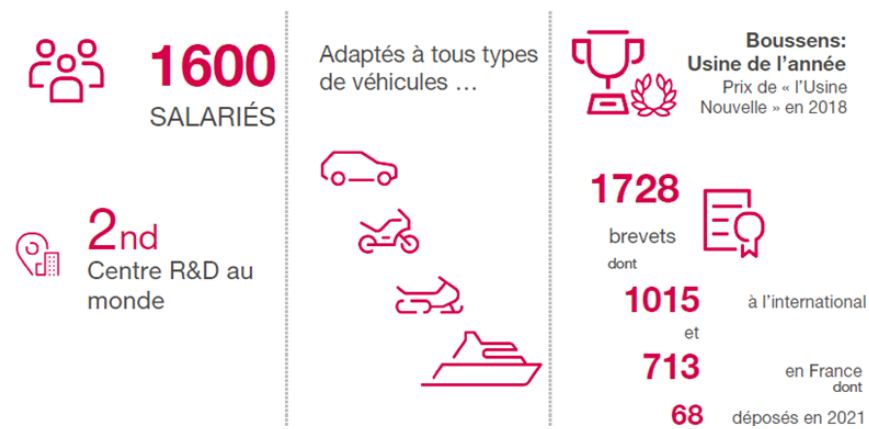
Source: Vitescho Technologies internal archives.

The company's objective is to develop innovative and efficient electrification technologies for all types of vehicles. Several areas of focus are studied, such as 48-volt electrification, electric drives and power electronics for hybrid and battery electric vehicles. As a pioneer in electrification, Vitesco technologies offers propulsion solutions for all types of electrified vehicles.

Vitesco Technologies provides parts and solutions for an entire electric vehicle as shown below:

Figure 3 – Parts and solutions provided by Vitesco Technologies for an entire electric vehicle.
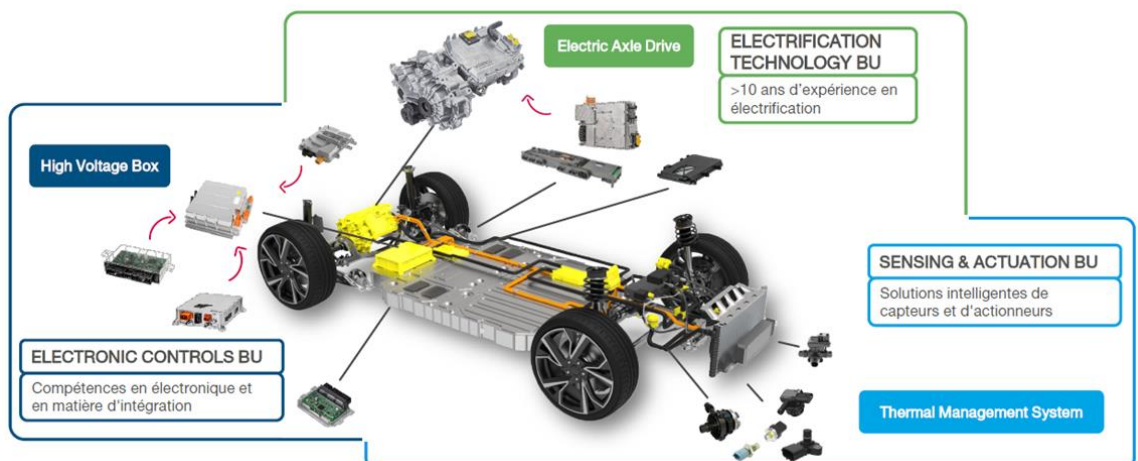
Source: Vitescho Technologies internal archives.

Thus, Vitesco Technologies proposes to develop solutions for the electrification of vehicles in order to reduce as much as possible the greenhouse gas emissions.

1.2   PROJECT BACKGROUD

The vehicle electrical system is defined by the following schematics:

Figure 4 – Vehicle electrical system architecture.
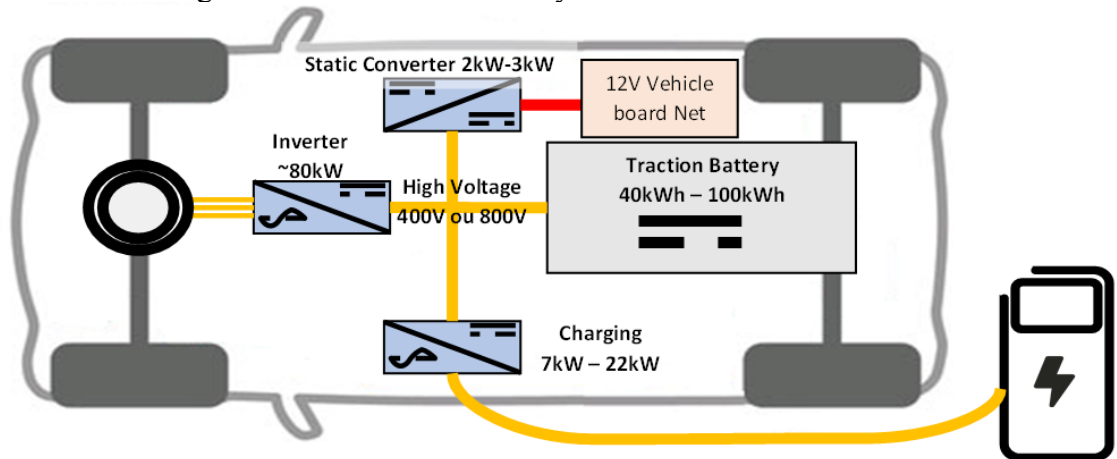
Source: Vitescho Technologies internal archives.

The Figure 4 show that the high voltage traction battery (400V or 800V) supply different static converters.

There is a DC/AC converter (Inverter on the diagram) passing from the DC voltage of the battery to the three-phase of the electric machine. The purpose of this converter is to drive the torque of the traction motor.

The low power DC/DC converter (Static Converter on the diagram) connect the traction battery to the vehicle's on-board network at 12 Volt. This converter allows to supply all the on-board system of the vehicle, such as infotainment system, vehicle auxiliaries and among others. To ensure the safety of the electrical appliances taking the 12 V voltage from the high voltage battery, there is a transformer in this converter to physically isolate the two circuits and thus protect the low voltage network from insulation error from the high voltage network of the car.

The last converter is the on-board charger (Charging on the diagram). The on-board chargers in cars are monodirectional or bidirectional static AC/DC converters. They convert AC electrical energy from the distribution network into DC electrical energy required by the traction battery.

The rest of this study will focus on the on-board charger.

1.2.1 Structure of an on-board charger on an electric vehicle

The structure of an on-board charger is composed of two conversion stages.

Figure 5 – Diagram of the converter.
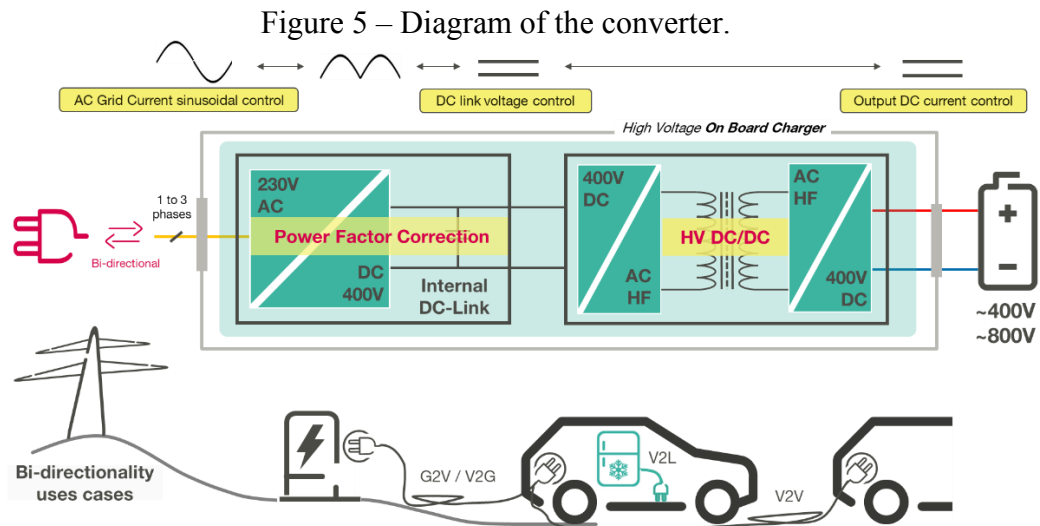
Source: Vitescho Technologies internal archives.

The first stage, called PFC (Power Factor Correction) allows to rectify the AC voltage of the network while guaranteeing a sinusoidal current absorption. It is usually a boost topology, the aim being to have a constant output voltage Vbus (DC-link) at 800V, which allows to decouple the two functions PFC and DC/DC.

The second stage, called DC/DC converter, regulates the output DC current in order to charge the battery. The DC/DC converter contains an isolation transformer to protect the internal network from possible insulation error coming from the grid network.

1.1 INTERNSHIP PROBLEMATIC

The internship problematic is situated at the internal DC-link. More specifically, the aim of the internship work, is to estimate the current value entering the DC/DC converter, showed by an red arrow at the Figure 5. As we already have measures at the input and output of the charger, will be of great use to estimate the current entering at the DC/DC.

There are three main reasons to estimate this current:

- It will be possible to know the DC/DC loss;
- The PFC and DC/DC performance can be monitored during life time;
- To better compensate disturbances with the voltage control loop at DC-Link.

The estimation will be done with a state observer called Kalman Filter. The choice of this state observer comes mainly from the fact that the Kalman Filter can combine several different data sources to achieve its estimation and it can take into account the uncertainties.

2 DEVELOPMENT AND IMPLEMENTATION

2.1   DC-LINK MODELING

2.1.1   Typical scheme

The B6's average value equations are based on the diagram below:

Figure 6 – Power Factor Correction model.
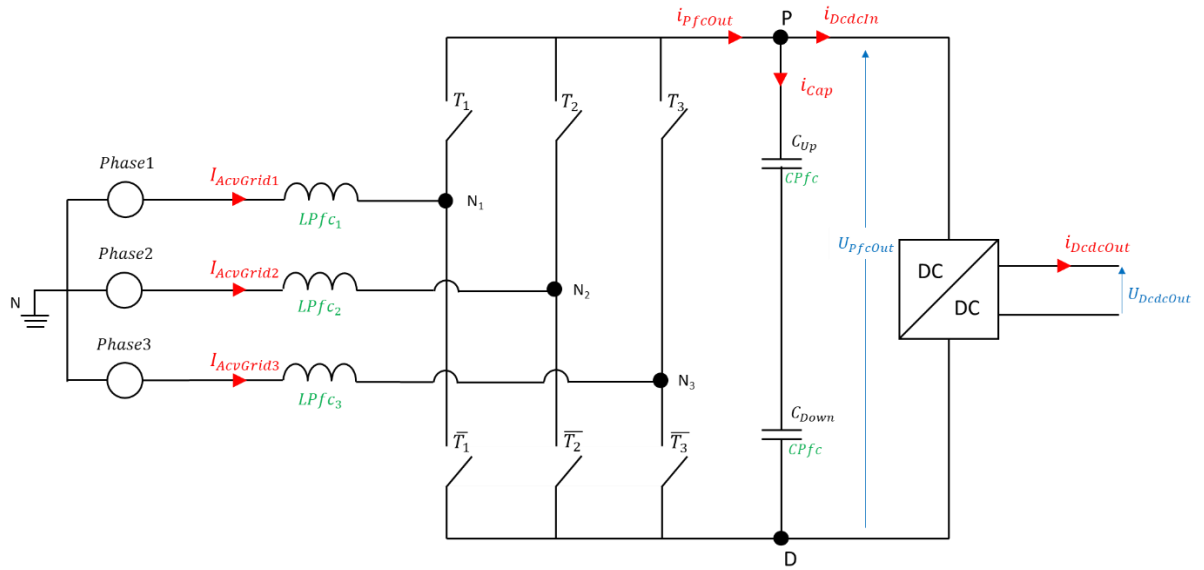
Source: Author.

Looking at this model and modeling it in equations, it will be possible to start the studies and simulations. For the current coming out of the PFC, the equation is given by the following expression:

$$i_{PfcOut} = \sum_x \alpha_x * I_{AcvGrid_x}$$

By the Kirchhoff's first law, it is possible to find the following equation:

$$i_{Cap} = i_{PfcOut} - i_{DcdcIn}$$

The equation of the current at the capacitor is:

$$i_{Cap} = \frac{C_{Pfc}}{2} \frac{d(U_{PfcOut})}{dt}$$

And finally, putting everything together, it is given the following equation modeling the PFC voltage:

$$\frac{C_{Pfc}}{2} \frac{d(U_{PfcOut})}{dt} = i_{PfcOut} - i_{DcdcIn} = \sum_x \alpha_x * i_x - i_{DcdcIn}$$

The DC link voltage is measured with an anti-aliasing first order filter, and it is:

- PFC output voltage: U_{PfcOut}.

2.2 STATE SPACE MODELING

2.2.1 Continuous state space model

As defined in the previous section the dynamic model of the B6 converter is given by the following equations:

$$i_{Cap} = i_{PfcOut} - i_{DcdcIn}$$

$$i_{Cap} = C \frac{dU_{PfcOut}}{dt}$$

$$\frac{dU_{PfcOut}}{dt} = \frac{1}{C} i_{PfcOut} - \frac{1}{C} i_{DcdcIn}$$

As the DC-link voltage is measured by a first order anti-aliasing filter, we obtain the following equations:

$$U_{PfcOutMes} = \frac{1}{1 + \tau s} U_{PfcOut}$$

$$U_{PfcOutMes} + \tau \frac{dU_{PfcOutMes}}{dt} = U_{PfcOut}$$

$$\frac{dU_{PfcOutMes}}{dt} = \frac{1}{\tau} U_{PfcOut} - \frac{1}{\tau} U_{PfcOutMes}$$

Considering $\tau = \frac{1}{\frac{\pi F_{SW}}{2}}$.

Passing to state space form:

$$\begin{bmatrix} \dot{U}_{PfcOut} \\ \dot{U}_{PfcOutMes} \end{bmatrix} = \begin{bmatrix} 0 & 0 \\ \frac{1}{\tau} & -\frac{1}{\tau} \end{bmatrix} \begin{bmatrix} U_{PfcOut} \\ U_{PfcOutMes} \end{bmatrix} + \begin{bmatrix} \frac{1}{C} & \frac{1}{C} \\ 0 & 0 \end{bmatrix} \begin{bmatrix} i_{Cap} \\ i_{DcdcIn} \end{bmatrix}$$

$$U_{PfcOutMes} = \begin{bmatrix} 0 & 1 \end{bmatrix} \begin{bmatrix} U_{PfcOut} \\ U_{PfcOutMes} \end{bmatrix}$$

The capacitance value C is the equivalent capacitance between C_{Up} and C_{Down}, given by the following equation:

$$C = \frac{C_{Up} \cdot C_{Down}}{C_{Up} + C_{Down}}$$

2.2.2 Discrete state space model

Now the system found above will be discretized. Starting with U_{PfcOut}:

$$C\frac{dU_{PfcOut}}{dt} = i_{PfcOut} - i_{DcdcIn}$$

Integrating:

$$U_{PfcOut} = \frac{1}{Cs}\left(i_{PfcOut} - i_{DcdcIn}\right)$$

Applicating the z-transform:

$$U_{PfcOut} = \frac{Ts}{C}\frac{1}{1-z^{-1}}\left(i_{PfcOut} - i_{DcdcIn}\right)$$

Managing the equations, it is given the $U_{PfcOut}(k+1)$ equation:

$$U_{PfcOut}(k+1) = U_{PfcOut}(k) + \frac{Ts}{C}i_{PfcOut}(k) - \frac{Ts}{C}i_{DcdcIn}(k)$$

Now passing to $U_{PfcOutMes}$:

$$U_{PfcOutMes} = \frac{1}{1+\tau s}U_{PfcOut}$$

Considering $\alpha = e^{\frac{-Ts}{\tau}}$ and applicating the z-transform:

$$U_{PfcOutMes} = \frac{1-\alpha}{1-\alpha z^{-1}}U_{PfcOut}$$

Managing the equations, it is given the $U_{PfcOutMes}(k+1)$ equation:

$$U_{PfcOutMes}(k+1) = \alpha U_{PfcOutMes}(k) + (1-\alpha)U_{PfcOut}(k)$$

This leads to the following discrete state space model:

$$\begin{bmatrix} U_{PfcOut}(k+1) \\ U_{PfcOutMes}(k+1) \end{bmatrix} = \begin{bmatrix} 1 & 0 \\ 1-\alpha & \alpha \end{bmatrix}\begin{bmatrix} U_{PfcOut}(k) \\ U_{PfcOutMes}(k) \end{bmatrix} + \begin{bmatrix} \frac{Ts}{C} & \frac{-Ts}{C} \\ 0 & 0 \end{bmatrix}\begin{bmatrix} i_{Cap}(k) \\ i_{DcdcIn}(k) \end{bmatrix}$$

$$U_{PfcOutMes}(k) = [0 \quad 1]\begin{bmatrix} U_{PfcOut}(k) \\ U_{PfcOutMes}(k) \end{bmatrix}$$

2.3   NOISE AND SYSTEM UNCERTAINTY

2.3.1   Measurement noise determination

The measured signal has two parts: the signal itself and the noise contained in it, as shown in the figure below. So, this noise must be considered in the studies to be done, and that is what will be covered in this topic.

Figure 7 – Signal and noise coming with it from the sensor.
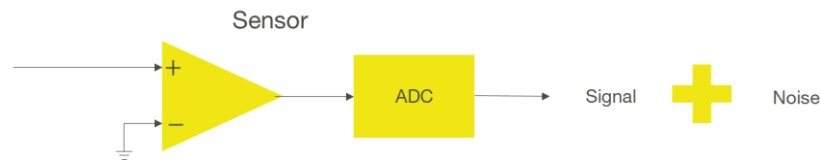
Source: Author.

To simulate the noise, it was used a random number generator, according to the 68-95-99.7 rule of statistics (2023).

The maximum noise of both current and voltage are explained at the next two subtopics.

2.3.1.1 Current noise

It was used 4 different set of measurements to define the current noise probability density: 400V Dc-link for 4kW and 5kW, and 600V Dc-link for 4kW and 5kW, giving 35000 samples.

Figure 8 – Current noise probability density.
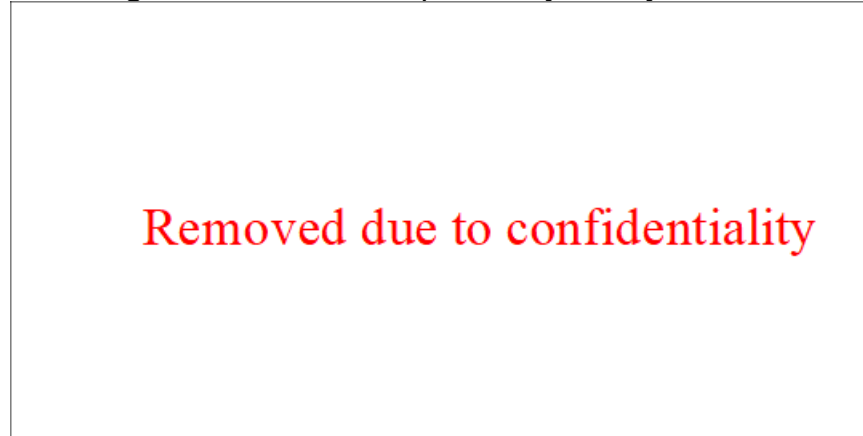
Source: Author.

Remark: All the histogram shown at this report are generated with Normalization and pdf argument.

The red line represents a gaussian distribution function. As the main part of all histograms are inside the gaussian law we could estimate that the noise is mainly gaussian. As the noise is gaussian, another time we see that we could use a Kalman filter to mitigate the noise on the B6 output voltage measurement.

Remark: The 6σ values will always be showed as a dashed line in this document.

2.3.1.2 Voltage noise

It was used several sets of measurements to measure the voltage noise probability density. Giving 23000 values.

Figure 9 – Voltage noise probability density.

Removed due to confidentiality
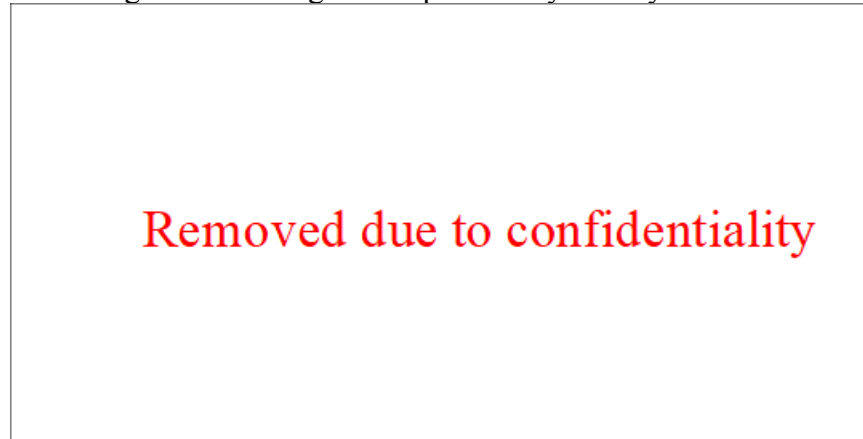
Source: Author
.

The red line represents a gaussian distribution function. The same way as saw for the current noise, as the main part of all histograms are inside the gaussian law we could estimate that the noise is mainly gaussian.

In the next section, this noise will be modelized as two different factors:

- **FacIAcvGridMes:** Responsible for modeling the current grid noise;
- **FacUPfcOutMes:** Responsible for modeling the voltage noise.
  Each factor is defined by the following expression: $Fac = N(1, \sigma)$.

2.3.2 System components uncertainty determination

The system has some types of uncertainty: at the current and voltage sensing, and a spread at the capacitors. All these uncertainties have a Gaussian law of distribution, and all values was taken at 6σ, it means that the values taken have a 0.000000197% (2 parts per billion) probability of occurrence.

2.3.2.1 Grid current sensor spread

For these studies, looking at the current, it was used a current sensor.

The picture bellow shows a specification extract:

Figure 10 – Current sensor manufacturer specifications extract.

Removed due to confidentiality
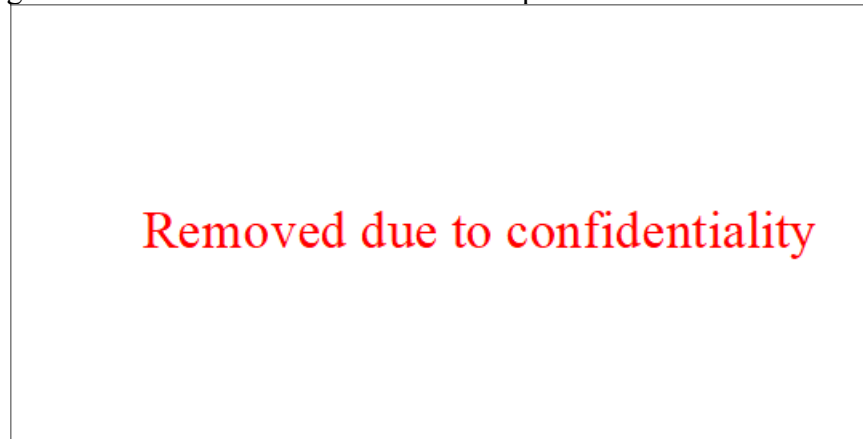
Source: Author.

The current accuracy is defined within a range of $\pm$X% at 6σ according to the value given by the manufacturer about the sensors and its normal law graphic is showed in the following figure:

Figure 11 – Current sensor spread probability density.

Removed due to confidentiality
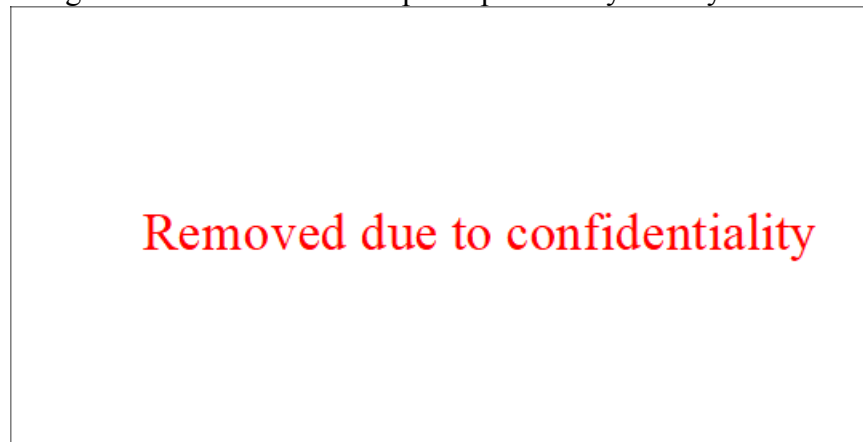
Source: Author
.

The majority of tests is done within a range of $\pm$X% at 6σ as mentioned, but in some cases, it was done within a range of $\pm$X% at 3σ to better understand the system behavior.

Finally, to represent the grid current sensor spread, it is used $FacIAcvGridMes$, defined at the following equations:

$$I_{AcvGrid} = I_{AcvGridRaw} \cdot FacIAcvGridMes$$
$$FacIAcvGridMes = N(1, \sigma)$$

2.3.2.2 DC-link Voltage sensor spread

Looking at the voltage, it was used a standard known setting. The voltage accuracy is defined within a range of $\pm X\%$ at 6σ and its normal law graphic is showed in the following figure:

Figure 12 – Current sensor spread probability density.
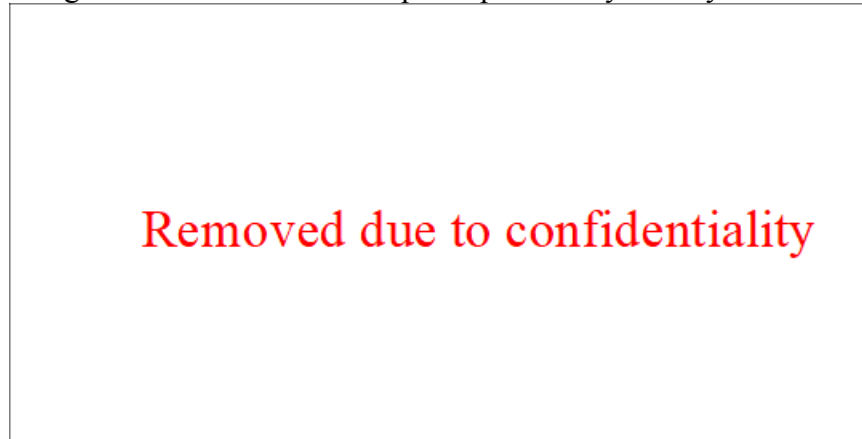
Source: Author.

Finally, to represent the voltage sensor spread, it is used $FacUPfcOutMes$, defined at the following equations:

$$U_{PfcOut} = U_{PfcOutRaw} \cdot FacUPfcOutMes$$

$$FacUPfcOutMes = N(1,\sigma)$$

2.3.2.3 DC-link Capacitor spread

We will consider the following DC-link capacitor as reference:

Figure 13 – Capacitor value spread probability density.
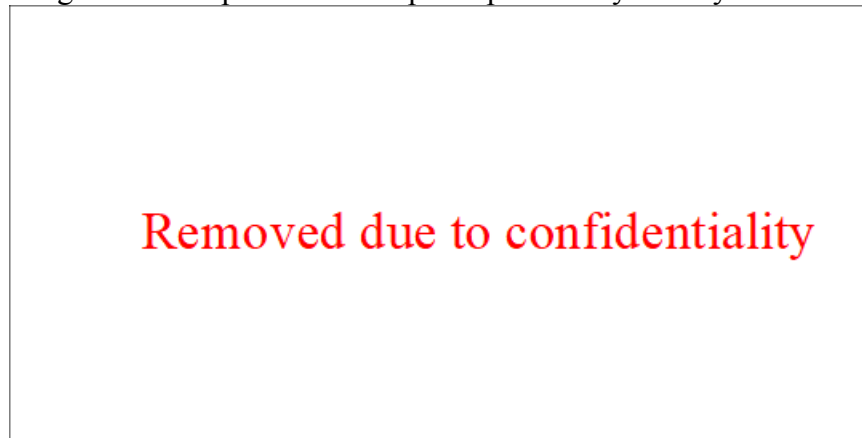
Source: Author.

Where $LSL = X * Target$ and $USL = X * Target$. Its standard deviation is done for a 6σ calculus. The capacitor spread at the simulation vary according to a factor within a range of $\pm X\%$.

2.4 DC/DC INPUT CURRENT OBSERVATION

As the noise and the components uncertainties are gaussian, a Kalman filter will be studied.

Reminder: A Kalman filter is defined by the following general algorithm:

Prediction:

$$\hat{x}_k^- = A\hat{x}_{k-1} + Bu_k$$
$$P_k^- = AP_{k-1}A^T + Q$$

Update:

$$K_k = \frac{P_k^- C^T}{CP_k^- C^T + R}$$
$$\hat{x}_k = \hat{x}_k^- + K_k(y_k - C\hat{x}_k^-)$$
$$P_k = (I - K_k C)P_k^-$$

With:

- **Q**: Process/estimated state noise covariance matrix;
- **R**: Measurement noise covariance matrix.

The Kalman Filter will have U_{PfcOut} as measure (y_k at the general algorithm) and i_{PfcOut} as input (u_k at the general algorithm). Within the Kalman filter block, the matrices A, B, and C obtained from the discrete state space model are used. i_{PfcOut} was rebuilt at this block in the same way as it was built as shown in section 2.1.

About the matrices R and Q. The matrix R is a constant of the same size as the input u_k.

Three methods will be studied to the DC-link current observation.

2.4.1 First method – Kalman Filter only

The objective of this Kalman Filter is to estimate the current i_{DcdcIn} that goes in the DC/DC converter, but the state space model found until now do not have a state of the current

to be estimated. This leads to the necessity to create an extended state space, that includes the current mentioned. To do this, it will be considered that the change of the current i_{DcdcIn} between each sample is very small:

$$i_{DcdcIn}(k+1) = i_{DcdcIn}(k)$$

This leads to the following extended discrete state space:

$$\begin{bmatrix} U_{PfcOut}(k+1) \\ U_{PfcOutMes}(k+1) \\ i_{DcdcIn}(k+1) \end{bmatrix} = \begin{bmatrix} 1 & 0 & \dfrac{-Ts}{C} \\ 1-\alpha & \alpha & 0 \\ 0 & 0 & 1 \end{bmatrix} \begin{bmatrix} U_{PfcOut}(k) \\ U_{PfcOutMes}(k) \\ i_{DcdcIn}(k) \end{bmatrix} + \begin{bmatrix} \dfrac{Ts}{C} \\ 0 \\ 0 \end{bmatrix} [\, i_{PfcOut}(k)]$$

$$U_{PfcOutMes}(k) = [0 \quad 1 \quad 0] \begin{bmatrix} U_{PfcOut}(k) \\ U_{PfcOutMes}(k) \\ i_{DcdcIn}(k) \end{bmatrix}$$

Finally, doing the observability test for this model found, it is assured that it is observable, and it is possible to pass to the implementation of the Kalman Filter at the Simulink model.

The Kalman Filter design stays:

Figure 14 – First method model.
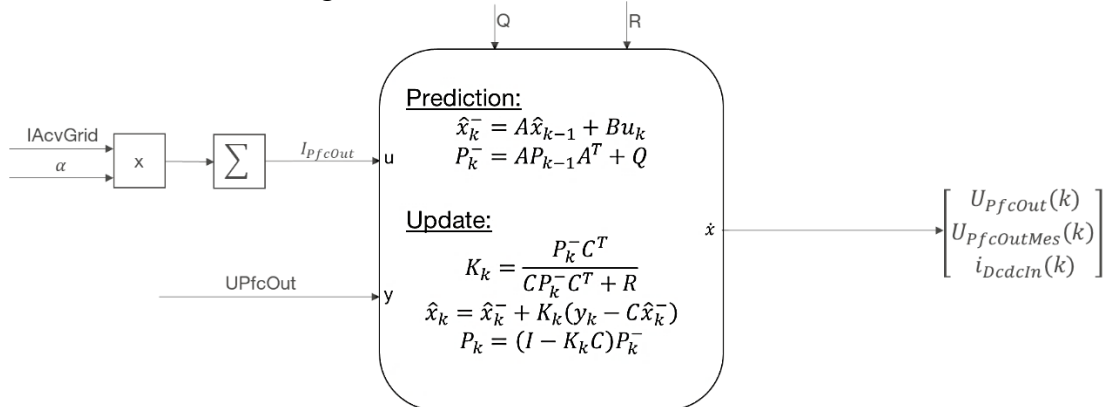
Source: Author.

The matrix Q is 3x3 diagonal, each element of the matrix has influence at a different state of the system:

$$Q = \begin{pmatrix} Q_{1,1} & 0 & 0 \\ 0 & Q_{2,2} & 0 \\ 0 & 0 & Q_{3,3} \end{pmatrix}$$

- $\mathbf{Q_{1,1}}$: variance/reliability of U_{PfcOut};
- $\mathbf{Q_{2,2}}$: variance/reliability of $U_{PfcOutMes}$;

- **Q$_{3,3}$**: variance/reliability of I_{DcdcIn}.

After, it will be studied a different method to estimate the current i_{DcdcIn}.

2.4.2   Second method – Sensor fusion

With this second method we want to enhance the 1st method estimation by considering the DC/DC output power measurement.

At this method, it will be done a probabilistic approach called sensor fusion (Bayesian law).

$$x3 = \frac{\sigma_2{}^2 x_1 + \sigma_1{}^2 x_2}{\sigma_1{}^2 + \sigma_2{}^2}$$

But before this approach, it is necessary to be introduced a new variable:

$$i_{outRaw}(k) = \frac{Pow_{DcdcOut}(k)}{U_{PfcOut}(k) \cdot Eff_{Dcdc}}$$

$Pow_{DcdcOut}$ is the power measured at the DC/DC converter output and Eff_{Dcdc} is the efficiency of the DC/DC, given by the following lookup table:

Figure 15 – DC/DC converter efficiency profile.

Removed due to confidentiality
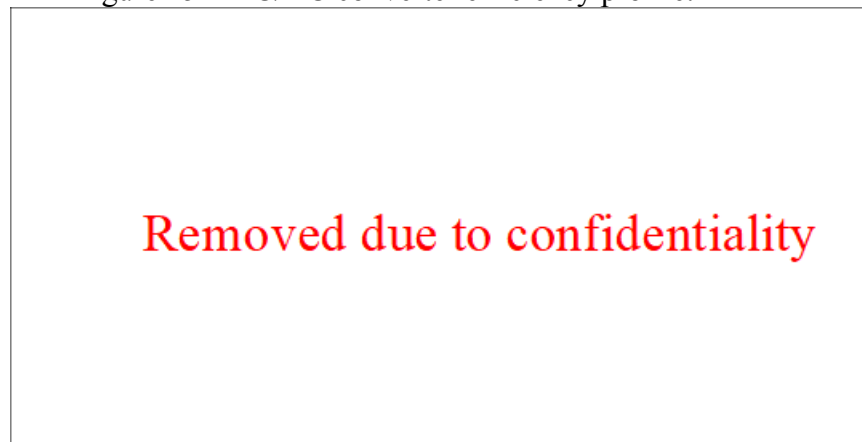
Source: Author.

Where $x2$ depends on the power $PowDcdc$ by $i_{DcdcInRaw}$, $x1$ equal to $i_{DcdcIn\_1st\_method}$ and $x3$ is the new estimated state i_{DcdcIn}:

$$x3 = \frac{\sigma_2{}^2 x_1 + \sigma_1{}^2 x_2}{\sigma_1{}^2 + \sigma_2{}^2} \implies i_{DcdcIn} = \frac{\sigma_2{}^2 i_{DcdcIn\_1st\_method} + \sigma_1{}^2 i_{DcdcInRaw}}{\sigma_1{}^2 + \sigma_2{}^2}$$

With σ_1 being the $i_{DcdcIn\_1st\_method}$ standard deviation, fixed at $\pm 5.2\%$ (or $\pm 2.6\%$ at 3σ case) that come from the grid current sensor studied previously. And σ_2 being the $i_{DcdcInRaw}$

standard deviation, fixed at $\pm 8\%$ that come from the DC/DC converter performance. The following figure show the 2nd method schematic:

Figure 16 – Second method model.

Source: Author.
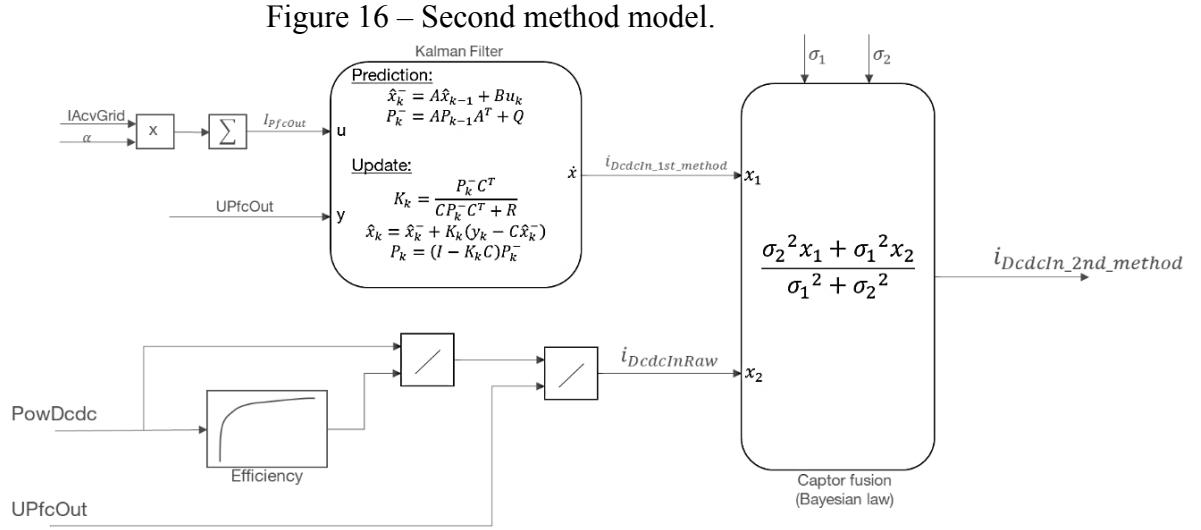
Finally, the last method to be studied is explained in the next section.

2.4.3 Third method – New State Space Model

With this Third method we want to enhance the method 1 estimation by considering the DC/DC output power measurement but here with a direct integration in the state space definition.

At this method, it is made some changes at the initial state space model. Initially, at the first state space model, it was used:

$$U_{PfcOut}(k+1) = U_{PfcOut}(k) + \frac{Ts}{C} i_{PfcOut}(k) - \frac{Ts}{C} i_{DcdcIn}(k)$$

But now instead of using i_{DcdcIn} as state, it will be replaced by $\Delta I(k) + i_{DcdcInRaw}(k)$ for modeling, arriving at the following expression:

$$U_{PfcOut}(k+1) = U_{PfcOut}(k) + \frac{Ts}{C} i_{PfcOut}(k) - \frac{Ts}{C} (\Delta I(k) + i_{DcdcInRaw}(k))$$

Where $\Delta I(k)$ is the variation of the current $i_{DcdcInRaw}$.

To solve this problem, similarly that done before, it will be considered that the change of the current ΔI between each step of the simulation is very small:

$$\Delta I(k+1) = \Delta I(k)$$

This leads to the following extended discrete state space:

$$\begin{bmatrix} U_{PfcOut}(k+1) \\ U_{PfcOutMes}(k+1) \\ \Delta I(k+1) \end{bmatrix} = \begin{bmatrix} 1 & 0 & -\frac{T_s}{c} \\ 1-\alpha & \alpha & 0 \\ 0 & 0 & 1 \end{bmatrix} \cdot \begin{bmatrix} U_{PfcOut}(k) \\ U_{PfcOutMes}(k) \\ \Delta I(k) \end{bmatrix} + \begin{bmatrix} \frac{T_s}{c} & -\frac{T_s}{c} \\ 0 & 0 \\ 0 & 0 \end{bmatrix} \cdot \begin{bmatrix} i_{Up}(k) \\ i_{DcdcInRaw}(k) \end{bmatrix}$$

$$U_{PfcOutMes}(k) = \begin{bmatrix} 0 & 1 & 0 \end{bmatrix} \cdot \begin{bmatrix} U_{PfcOut}(k) \\ U_{PfcOutMes}(k) \\ \Delta I(k) \end{bmatrix}$$

Where:

$$i_{DcdcIn}(k) = \Delta I(k) + i_{DcdcInRaw}(k)$$

The following figure show the 3rd method schematic:

Figure 17 – Third method model.

Source: Author.
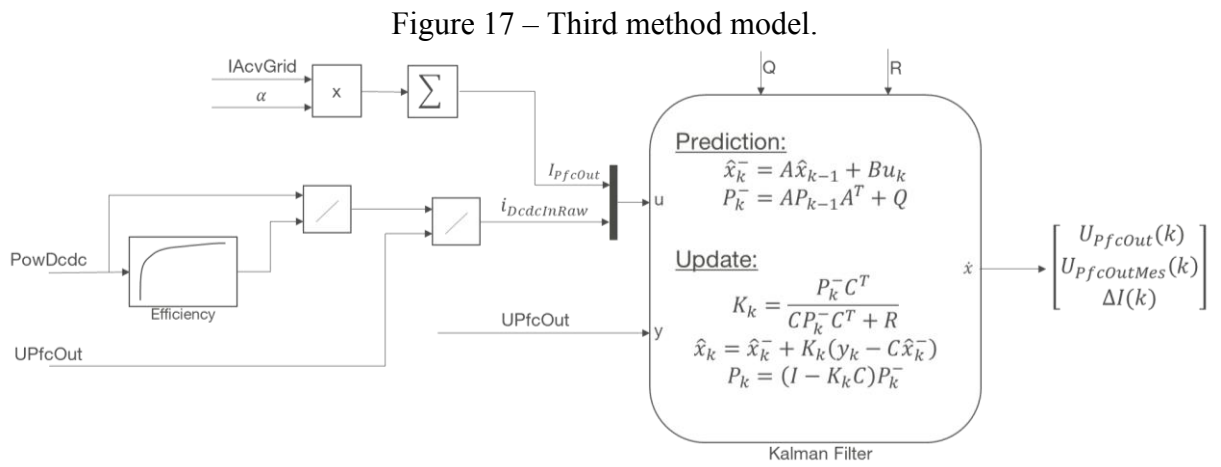
Now all three methods are defined and then it is needed to evaluate the performances of each one.

2.5   CORNER CASE STUDY

To arrive at a more consistent result and to have a system working even in the worst scenarios, it will be done a corner case study (2022), changing the parameters: DC/DC Power, grid current sensing spread, Dc link voltage sensing spread and capacitor spread.

The tests will be based on the permutation of the four values showed at the following schematic:

Figure 18 – Different factors extremity values.
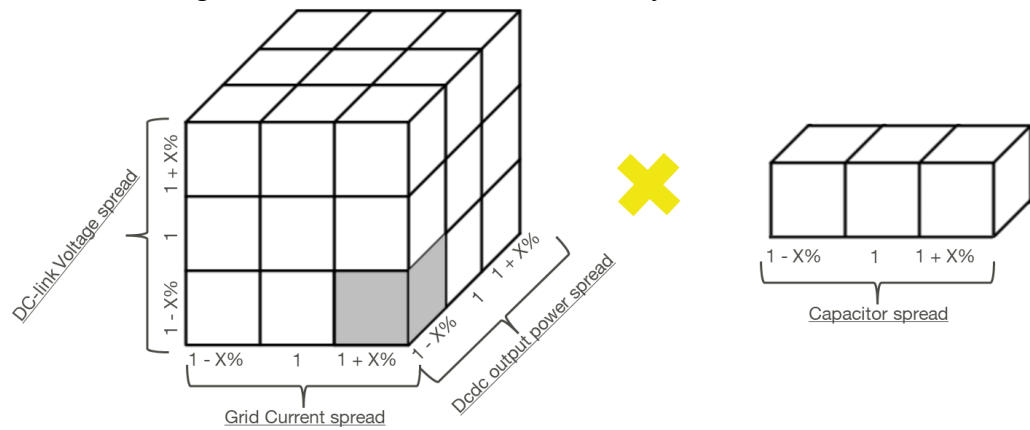
Source: Author.

It will give 81 different simulations. After it is explained how the evolution of the studies was done, starting with the definition of the metrics and parameters of the system and ending with the Monte Carlo study.

2.6   PROCESS WORKFLOW

To simplify the explanation of how all studies were made, the following flowchart is used.

Figure 19 – Process workflow flowchart.
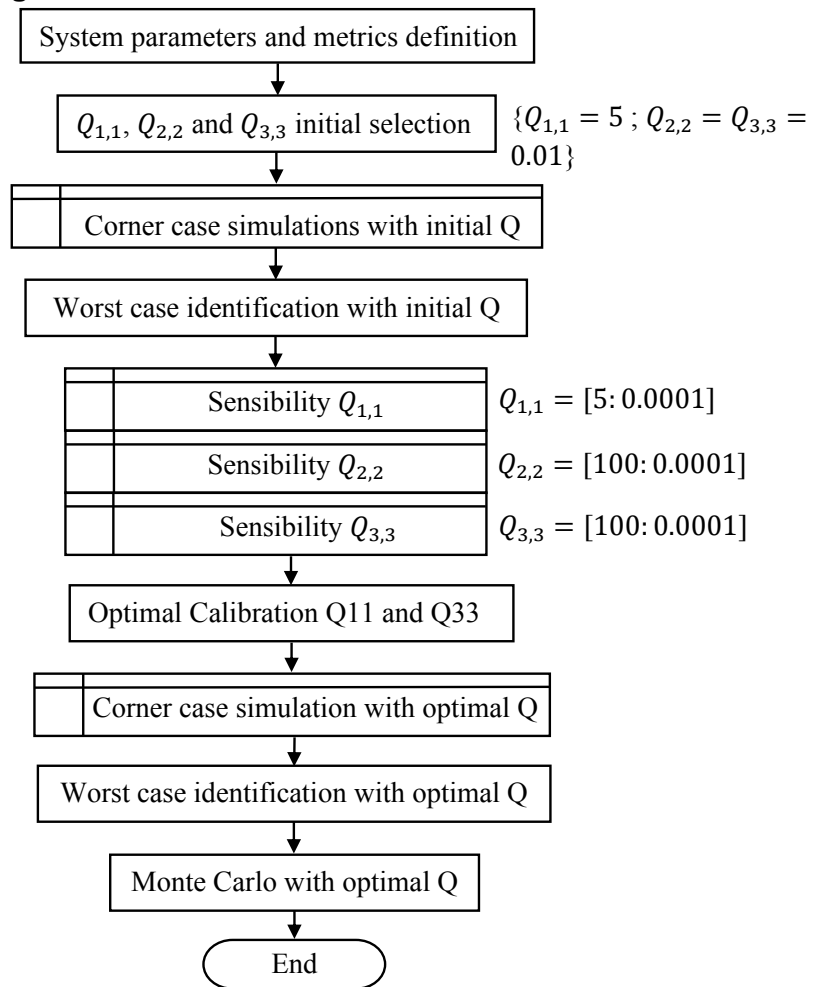
Source: Author.

The process to be studied is a multivariable system, so this makes the drawing of conclusions more complex. For this reason, to limit the number of simulations, it will be found two instances for the worst-case parameters.

In this way, firstly it is defined the system parameters and the metrics to be used, then it is chosen a standard $Q_{1,1}$, $Q_{2,2}$ and $Q_{3,3}$ to have initial values to start the study, passing by a corner case study and finding a worst-case parameter configuration.

Before continuing, it is needed to search the best configuration for the Q matrix, so it is taken these worst-case parameters and studied the sensibility of $Q_{1,1}$, $Q_{2,2}$ and $Q_{3,3}$ in a chosen large range and concluding that $Q_{1,1}$ and $Q_{3,3}$ have the most impact on the system, while $Q_{2,2}$ has negligible impact on the system.

Thanks to this sensibility analysis, an optimal solution search for $Q_{1,1}$ and $Q_{3,3}$ is conducted.

Finally, a second Corner Case is done with optimal Q matrix, finding another worst-case parameter configuration, now for the system performance study.

Then a Monte Carlo study is done to get results closer to the reality about the system uncertainty and noise.

2.7 POWER PROFILE DEFINITION

In order to assess the performances, two power profiles are defined.

2.7.1 Active power

The power profile used at this study is showed at the following graphic. Starting at zero and going until XkW, increasing the power value following a ramp profile.

Figure 20 – Active power profile.

Removed due to confidentiality
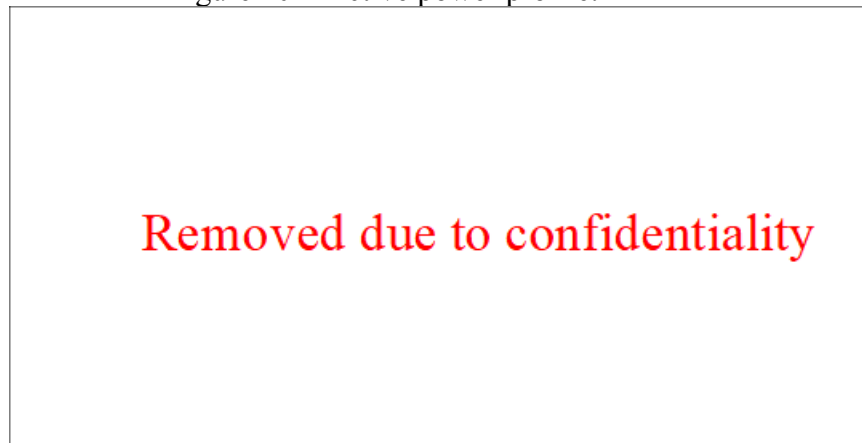
Source: Author.

2.7.2 Reactive power

Another time, to get closer to reality, it is necessary to include the reactive power to the system and look if the Kalman Filter continue to do its works as it is supposed to. The reactive power was included as the way showed at the following graphic, decreasing the active power defined before and injecting the reactive power, maintaining the total apparent power at XVA:

Figure 21 – Active and reactive power profile.

Removed due to confidentiality
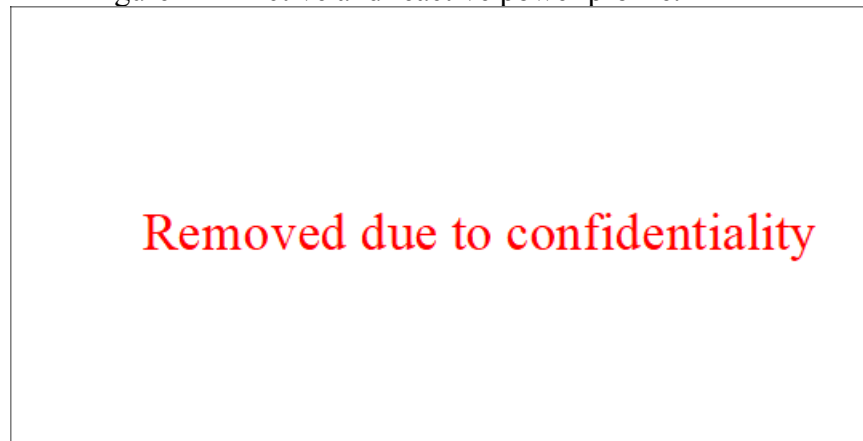
Source: Author.

As the power profile showed at the previous subsection, the reactive power has a ramp profile, starting at 0.3 second of simulation and going from zero to $XVAR$.

Now it is necessary to define the system performances criteria to be possible to compare each simulation.

2.8 PERFORMANCE'S CRITERIA DEFINITION

It is defined three zones (showed in the next graphic) to measure and compare:

- **1)** Beginning transitory: [First Zone];
- **2)** Final transitory: [Second Zone];
- **3)** Steady state: [Steady Zone].
  The current profile is given by the following graphic:

Figure 22 – Current profile and the zones used to measure and compare the results.

Source: Author.

Each interval was chosen as big enough to get enough data and small enough to get accurate data:

- **First Zone (1):** $[0.36\ s, 0.39\ s]$;
- **Second Zone (2):** $[0.70\ s, 0.73s\ ]$;
- **Steady Zone (3):** $[1.46\ s, end]$, where $end = 1.50\ s$.

Now zooming in at the second zone (final transitory regime), it is possible to see at the following graphic that the estimated current has an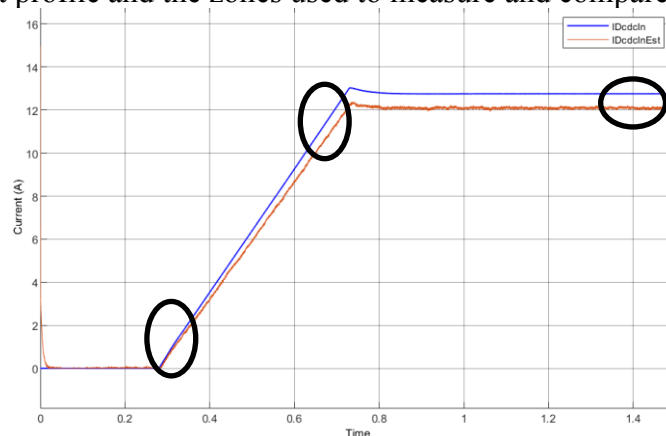 error to be calculated regarding the reference and it have also a noise. Both criteria defined will be used with the purpose to judge the system response.

Figure 23 – Current profile and the zones used to measure and compare the results.
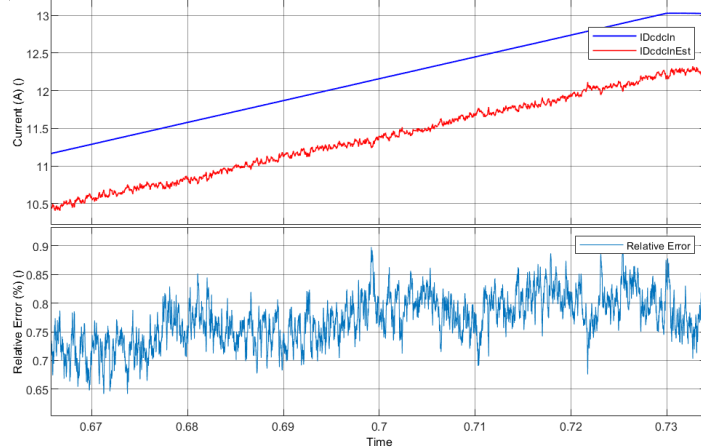
Source: Author.

To measure the system performance, it was used two different criteria:

Relative error (2020): To be possible to compare the estimated value with the ideal value:

$$Relative\ Error = mean\left(\frac{100 * (Mesure - Reference)}{Reference}\right)$$

Signal-to-noise ratio (SNR) (2023): To measure the quality of the estimation in term of noise content:

$$SNR = \frac{P_{Signal}}{P_{Noise}}$$

With all system configuration defined, now it will be searched the worst parameters configuration.

2.9   WORST CASE PER METHOD

As a product of the corner case study mentioned before, it was found the worst-case parameters between all 81 simulations in each method:

First method:

FacPowDcdcMes	FacIAcvGridMes	FacUPfcOutMes	FacCPfc
X1	X2	X3	X4

Table 1: First method worst case parameters.

Second method:

FacPowDcdcMes	FacIAcvGridMes	FacUPfcOutMes	FacCPfc
X1	X2	X3	X4

Table 2: Second method worst case parameters.

Third method:

FacPowDcdcMes	FacIAcvGridMes	FacUPfcOutMes	FacCPfc
X1	X2	X3	X4

Table 3: Third method worst case parameters.

These worst-case parameters will be used to obtain the corner case results, showed at the section 11.1 of this document.

2.10   CALIBRATION OPTIMIZATION

2.10.1 The R matrix

The Kalman Filter R matrix represents the reliability at the measure y and will be constant at the three different methods to be studied. In that case, it is a constant given by $R = (\frac{X}{6})^2$:

- **XV** → X% of $800V$ at 6σ from the voltage sensor;
- **XV** → Voltage measure noise;
- The division by 6 because it is all at a gaussian law at 6σ.

2.10.2 Recursive Q Matrix search for optimal value

After the implementation of the Kalman Filter, the next step consists in optimizing the calibration of the Kalman filter Q matrix. For this, it is needed to do several numbers of simulations with the same variation of parameters previously studied at chapter 8 of this document. The simulation of several different parameters configurations was made for the first and third method. Obtaining several possible solutions by respecting the specifications:

- Current Transitory [First and Second Zone]: Less than X% of relative error and $SNR > 10$;
- Current Steady State [Steady Zone]: Less than X% of relative error and $SNR > 10$;
- Voltage Steady State [Steady Zone]: Les than X% of relative error and $SNR > 10$.

The process to do a recursive search for the optimal value of parameters is showed by the following flowchart:

Figure 24 – Recursive search for optimal Q matrix flowchart.

Removed due to confidentiality
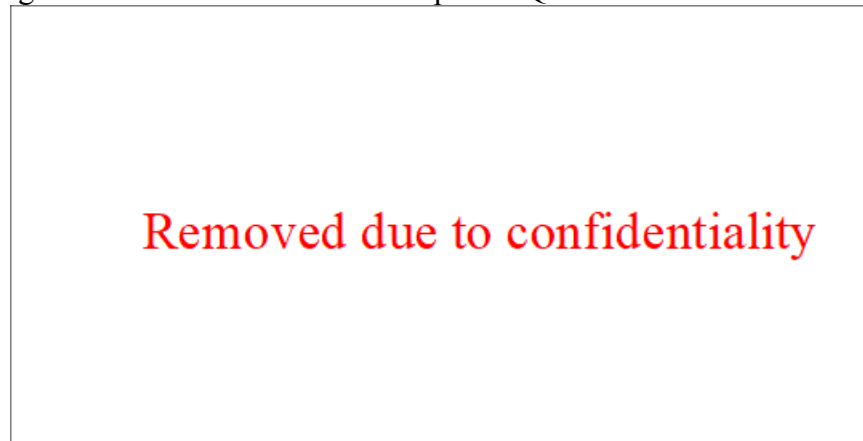
Source: Author.

At end of swipe based on the resulting table an optimal set of solution of $Q_{1,1}$ and $Q_{3,3}$ is selected based on our criteria define above.

2.10.2.1   First method best parameters

The function *parallelplot* creates a parallel coordinates plot from a determined table result. Each line in the plot represents a row in the table, and each coordinate variable in the plot corresponds to a column in the table.

Doing the research mentioned at this section, at the 1st method, and looking at the parallel coordinates data result shown ai the next Figure:

Figure 25 – Parallelplot used to find the optimal Q matrix solution for the first method.

Removed due to confidentiality
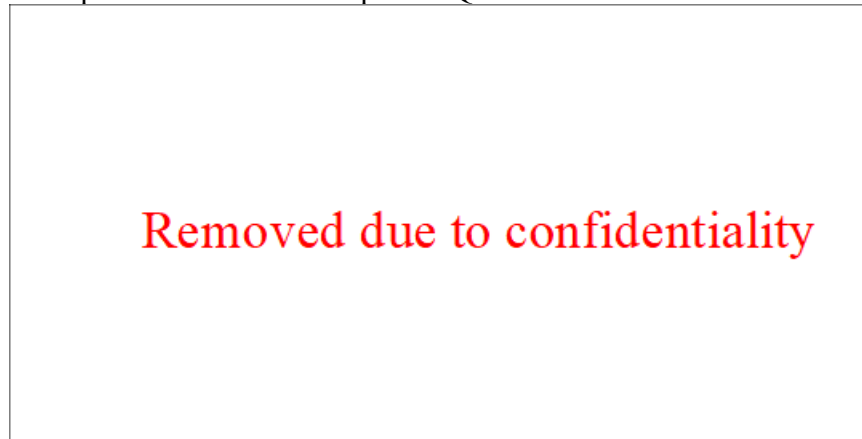
Source: Author.

It is found the Q matrix with its best values, as shown below:

$$Q = \begin{pmatrix} X & 0 & 0 \\ 0 & X & 0 \\ 0 & 0 & X \end{pmatrix}$$

2.10.2.2   *Third method best parameters*

For the 3rd method it was done in the same way as mentioned at the 1st method section. So, the given parallel plot is:

Figure 26 – Parallelplot used to find the optimal Q matrix solution for the third method.

Removed due to confidentiality
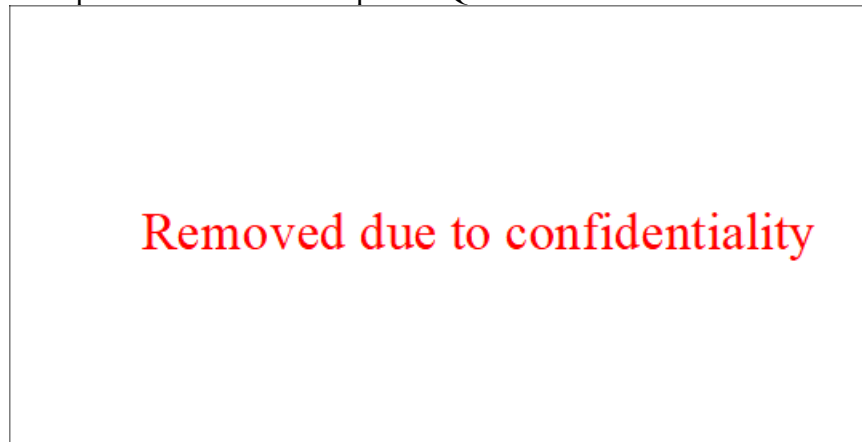
Source: Author.

Finding the following Q matrix with its best values:

$$Q = \begin{pmatrix} X & 0 & 0 \\ 0 & X & 0 \\ 0 & 0 & X \end{pmatrix}$$

2.11   TEST RESULT

Now based on the identified optimal Q matrix calibration we could evaluate the performances of the methods.

2.11.1 Corner case results

A corner case (or pathological case) involves a problem or situation that occurs only outside normal operating parameters, specifically one that manifests itself when multiple environmental variables or conditions are simultaneously at extreme levels, even though each parameter is within the specified range for that parameter.

It was done a corner case study with all 3 methods mentioned before and obtained the table shown below:

Figure 27 – Corner case results. Each line represents a different method and each column represents a different criteria.
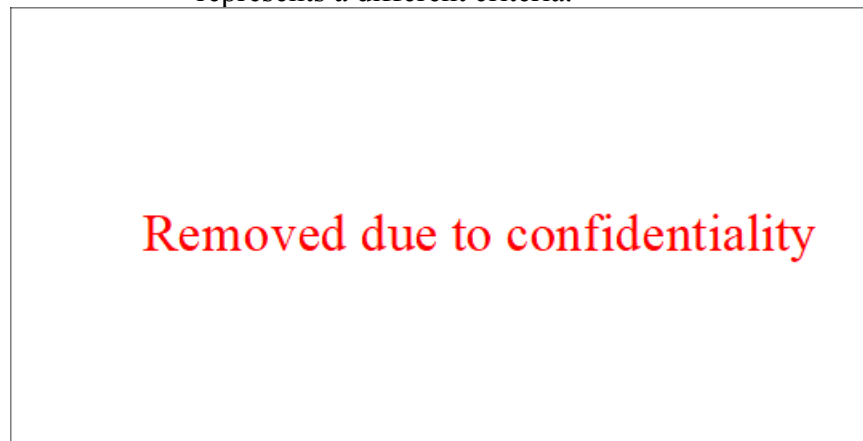
Source: Author.

Looking at the relative error, its minimum is X%, this X% is directly linked to the grid current sensor accuracy. Indeed, the accuracy of the estimated current cannot be lower than the accuracy of the grid current at the entry.

Looking at the SNR, all the Corner Case values are above 10 (criteria defined before).

Looking at the Corner Case result, in some cases the relative error do not respect our criteria. This happens because the optimum Q matrix found is not globally optimal, it is only locally optimal. And later, solutions to this problem will be proposed.

Therefore, looking at the corner case results shown in the graphs above, the methods studied do not meet the requirements for the relative error imposed in section 9.3. So in order to have a better view of the performances a Monte Carlo simulation is conducted.

Remark: The relative error at the first zone is worse than the other zones, due to the transient of the Kalman Filter.

2.11.2 Monte Carlo results

Monte Carlo methods, or Monte Carlo experiments, are a broad class of computational algorithms that rely on repeated random sampling to obtain numerical results. The underlying concept is to use randomness to solve problems that might be deterministic in principle.

The Monte Carlo method require a lot of simulation, to limit the number of simulations, it is used two steps:

- Firstly, it will be done a partial Monte Carlo study, swiping only $FacPowDcdcMes$ and $FacIAcvGridMes$, with more than 10000 simulations per method.
- Secondly, it will be done a complete Monte Carlo study only with the 1st method to confirm the result saw at the Partial Monte Carlo. Swiping the parameters FacIAcvGridMes, $FacCPfc$ and FacUPfcOutMes, maintaining $FacPowDcdcMes = 1$ (we will see in the next part that this factor does not impact the simulation result). This represents $45x45x45 = 91125$ simulations.

2.11.2.1   Partial Monte Carlo study

At the first figure, it was used $FacPowDcdcMes = 1$ for the 1st method and this same factor was swiped for the rest of the methods. The factor $FacIAcvGridMes$ was swiped for all methods and the rest of factors presented before (FacCPfc and FacUPfcOutMes) were kept constant equal to one.

Figure 28 – Partial Monte Carlo results with unitary FacPowDcdcMes for the first method. Each line represents a different method and each column represents a factor or the relative error for a given zone.

Removed due to confidentiality
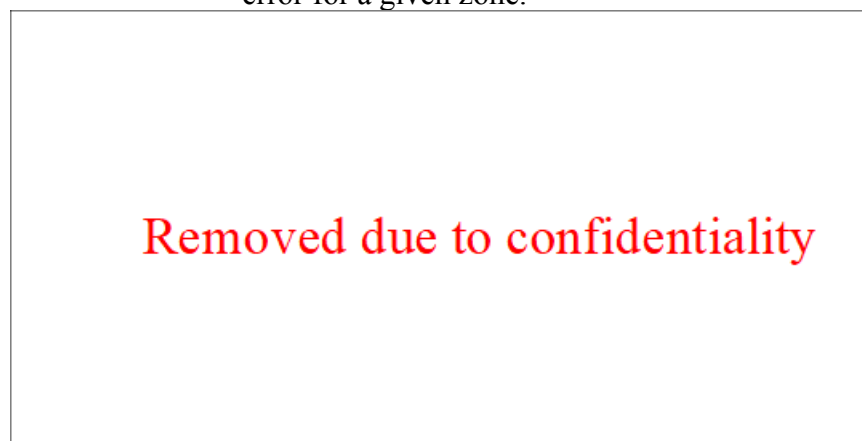
Source: Author.

But to be sure that the *FacPowDcdcMes* does not have an important impact at the 1st method, it was also used *FacPowDcdcMes* following a normal law of distribution as parameter to the simulation and obtained the results showed above. Swiping the factors *FacPowDcdcMes* and *FacIAcvGridMes*, and keeping the other two factors fixed.

Figure 29 – Partial Monte Carlo results with all factors following a normal law.

Removed due to confidentiality
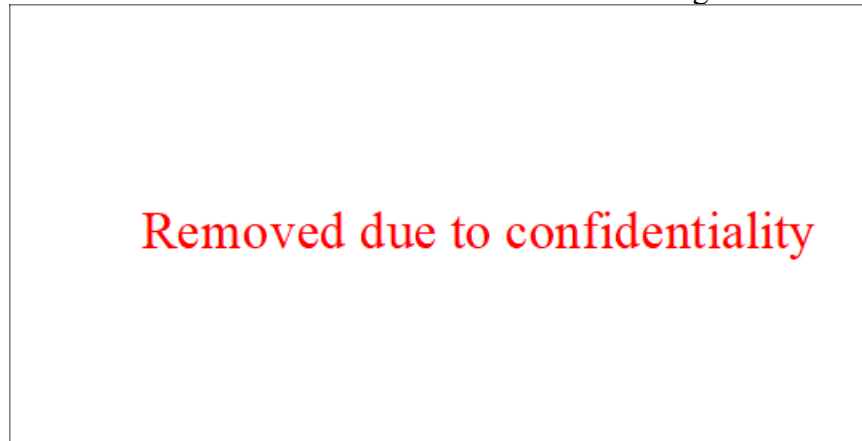
Source: Author.

If we look at the Corner Case in the previous section, the conclusion is that the results are not so satisfactory because the relative error is greater than desired. Now looking at the Monte Carlo results, the conclusion is different, because now we have an approach closer to reality, where extreme cases happen infrequently.

The table below represent the 6σ values reached by each method:

Figure 30 – 6σ value reached for each method.

Removed due to confidentiality
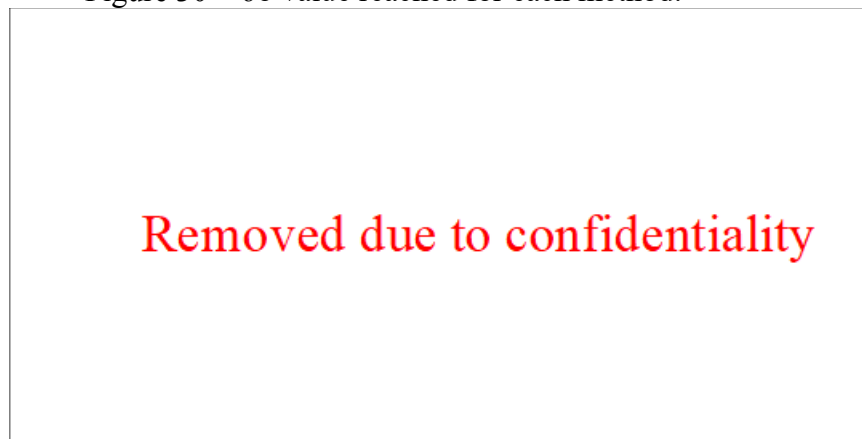
Source: Author.

Looking at the table above, it is possible to see that the 2nd method always meets the specifications, but the 1st and 3rd do not.
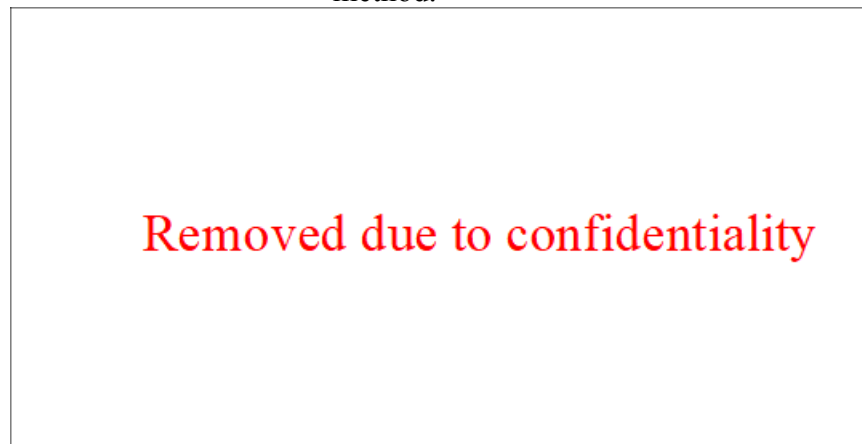
In the tables below we are looking for which sigma value the 1st and 3rd method meet the criteria.

Figure 31 – Maximum number of sigma to stay within the defined criteria for the 1st and 3rd method.

Removed due to confidentiality

Source: Author.

For the 1st method, the maximum sigma limit is reached at 4,5σ, meaning that 99.999320% of the cases are covered. After, for the 3rd method, the minimum sigma limit is reached at 4σ, meaning that 99.993666% of the cases are covered.

Doing this analysis, with all 3 methods it is possible to cover 99.993666% of cases (representing 4σ of the 68-95-99.7 rule).

Again, as concluded by looking at the results of the Corner Case study, we see that the calibration of the Q matrix used is not optimal. And still looking at the Monte Carlo study, it is possible to see that the values found and used in the Corner Case study are at the extremes of the 6σ zone.

So once again it is shown that the system has a good estimation, even if the Corner Case result shows otherwise in a first time.

Nextly it will be done a complete study with Monte Carlo method.

2.11.2.2   Complete Monte Carlo study

Now it will be done a complete Monte Carlo study with the 1st method Kalman Filter configuration, where it will be changed the factors $FacIAcvGridMes$, $FacCPfc$ and $FacUPfcOut$ following a normal law with the same number of points (45 points each one).

Figure 32 – Complete Monte Carlo results. The first lines are the factors varied and the second line are the relative error for a given zone.
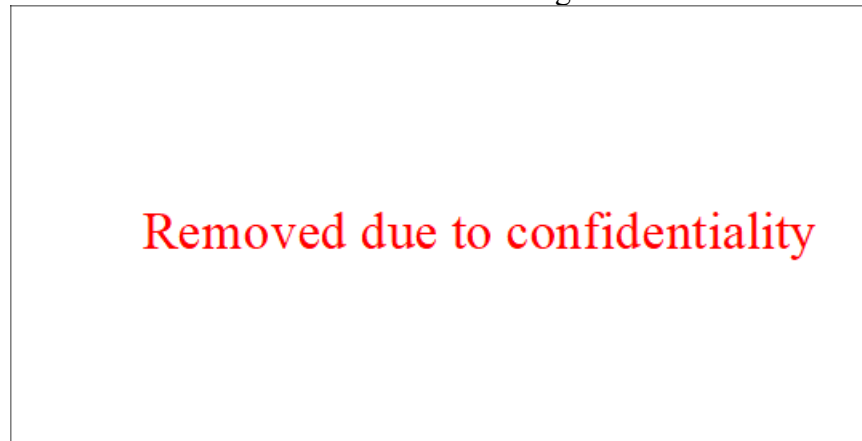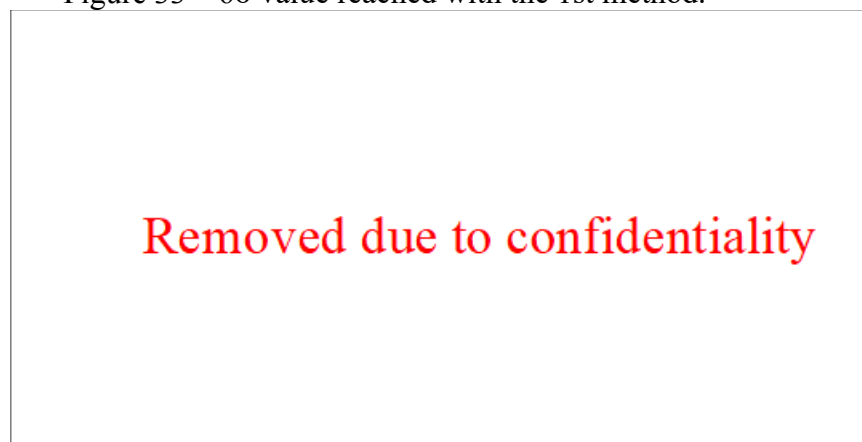

Source: Author.

Justifying the motivation to do a complete Monte Carlo study only with the 1st method. This method was chosen because $FacPowDcdcMes$ does not have a considerable influence on it, so it is one less factor to deal during the study, significantly reducing the number of simulations and thus the time of simulation. Because, when doing a Monte Carlo study, the consumption of computer processing grows up too quickly.

The table below represent the 6σ values reached by each method:

Figure 33 – 6σ value reached with the 1st method.

Source: Author.

Looking at the table above, it is possible to see that the 1st method at a complete Monte Carlo study does not always meets the specifications.

In the table below we are looking for which sigma value the 1st method meets the criteria.

Figure 34 – Maximum number of sigma to stay within the defined criteria for the 1st method.
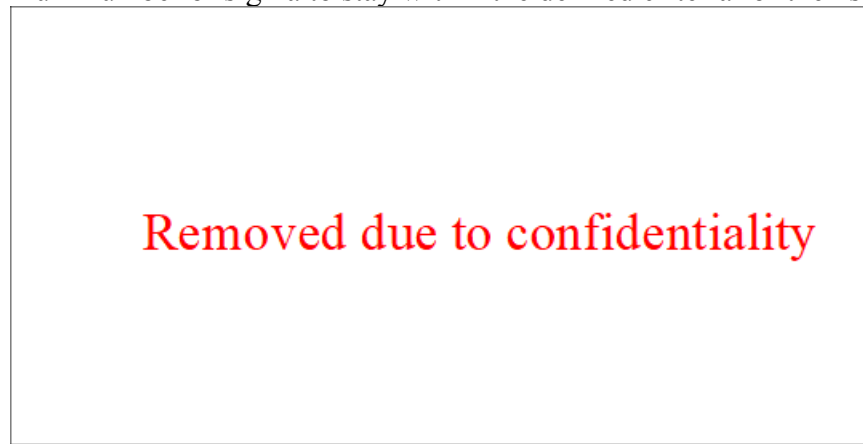
Source: Author.

For the 1st method, the minimum sigma limit is reached at 4,4σ/4,5σ, meaning that at least 99.999810% of the cases are covered.

Finally, another time with the Monte Carlo study, it is possible to define that the Kalman Filter does a good estimation. The relative error in the steady state (rightmost graph) is centered near X% and the relative error in the transitory regime is centered close to X%.

2 CONCLUSION

Looking predominantly at the relative errors, it is possible to conclude that the 2nd method of Kalman Filter adjustment is the one with the most satisfactory results, followed by the 1st method and after by the 3rd method.

About the memory and CPU cost, it can be classified from the cheaper to the expensive by the following expression: 1^{St} method $> 2^{nd}$ method $> 3^{rd}$ method.

Moreover, about the way in which the optimal calibration is calculated, the way used does not find the optimal global solution, because the worst case is constantly changing according to the Q matrix, then the Q matrix found is locally optimal only.

Looking at the Monte Carlo, it is possible to see that the system requirements imposed in section 9.3 are met at least in 99.993666% (4σ limit) of all cases.

Moreover, for a future work, there are two different steps to be taken:

1. Conduct a study on the sensitivity of the state observer to the sampling period. So far, it has been used as a basis XkHz frequency and then it can be studied at XkHz,XkHz or even lower (near XkHz), and see if an accurate estimation is still obtained;
2. New method that gives us a global optimization of the Q matrix that covers the extremes outside the 6σ zone looking at Monte Carlo results. Trying to obtain, even in these cases, an accurate estimation.

Finally, the work done during the internship was of great importance to reinforce my choice of doing the ACISE course at ENSEEIHT. I had the opportunity to apply in practice the knowledge learned in class and laboratory, from the mathematical basis to the more in-depth knowledge of engineering, such as the Kalman Filter itself.

Moreover, doing this internship at Vitesco Technologies gave me a first experience of working in a large company. It was very important for me to close the study cycle at ENSEEIHT and start a new cycle, inserting myself in the engineering job market. And giving me the certainty that I want to work in the engineering area in my professional career.

3 BIBLIOGRAPHY

2023. 68–95–99.7 rule. [Online] 23 de May de 2023. [Citado em: 05 de June de 2023.] https://en.wikipedia.org/wiki/68%E2%80%9395%E2%80%9399.7_rule.

2022. Corner case. [Online] 26 de January de 2022. [Citado em: 05 de June de 2023.] https://en.wikipedia.org/wiki/Corner_case.

2020. Relative error. [Online] 05 de November de 2020. [Citado em: 05 de June de 2023.] https://fr.wikipedia.org/wiki/Erreur_relative.

2023. Signal-to-noise-ratio. [Online] 29 de May de 2023. [Citado em: 05 de June de 2023.] https://en.wikipedia.org/wiki/Signal-to-noise_ratio.